Spectrum of neutral helium in strong magnetic fields

Matthew D. Jones and Gerardo Ortiz
Theoretical Division, Los Alamos National Laboratory, Los Alamos, New Mexico 87545

David M. Ceperley
Department of Physics and National Center for Supercomputing Applications, University of Illinois at Urbana–Champaign
1110 West Green Street, Urbana, Illinois 61801

(Received 10 November 1998)

We present extensive and accurate calculations for the excited-state spectrum of spin-polarized neutral helium in a range of magnetic field strengths up to 10^{12} G. Of considerable interest to models of magnetic white dwarf stellar atmospheres, we also present results for the dipole strengths of the low-lying transitions among these states. Our methods rely on a systematically saturated basis set approach to solving the Hartree-Fock self-consistent field equations, combined with an ''exact'' stochastic method to estimate the residual basis set truncation error and electron correlation effects. We also discuss the applicability of the adiabatic approximation to strongly magnetized multielectron atoms. [S1050-2947(99)02504-4]

PACS number(s): 32.60.+i, 31.10.+z, 97.10.Ld, 95.30.Ky

I. INTRODUCTION

The electronic structure of simple atomic systems in strong external fields remains poorly understood, despite considerable theoretical effort. These systems are of critical importance in certain stellar environments, in which very large magnetic fields have been inferred [1]. A detailed knowledge of the spectra of light atoms (presumed to dominate the atmospheres of compact stellar remnants) subjected to intense magnetic fields would enable both observers and theorists to better refine their understanding of these astrophysical objects. Unfortunately, only the spectrum of hydrogen has been adequately treated thus far, by Rosner *et al.* in 1984 [2]. This detailed work on hydrogen has been successfully applied to the observed spectra [3] from many magnetic white dwarf stars, but several stars remain in which the spectra cannot be accounted for by hydrogen [4], and in which the determination of the strength and configuration of the stellar magnetic field would be greatly aided by precise calculations of the spectrum of the next lightest element, neutral helium.

The difficulty in theoretically treating atoms in strong magnetic fields lies in the fact that magnetic and Coulomb forces are of nearly equal importance; neither can be treated as a perturbation of the other. In the uniform magnetic fields that we consider in this work (assumed to lie in the z direction), this difficulty translates into a competition between the cylindrical symmetry of the applied magnetic field, and the spherical symmetry of the Coulomb interactions. An often applied approximation is the adiabatic approximation [5], in which the electronic orbital is assumed to be a product of a Landau level [3] for the direction transverse to the magnetic field (in $\rho^2=x^2+y^2$) and a longitudinal function (in z) basically determined by the Coulomb interactions.

Several studies have recently addressed the electronic structure of helium atoms subjected to strong magnetic fields. Most works have examined only the lowest electronic states using Hartree-Fock (HF) [6–8] and variational [9,10,20] methods. To be predictive of observed stellar spectra, however, many excited states are required, not only the lowest atomic state for a given symmetry. These excited states must also be determined with sufficiently high accuracy to distinguish the dominant absorption features found in observed stellar spectra. Several recent attempts have been made to solve the HF self-consistent field (SCF) equations for the spectrum of magnetized helium. Thurner *et al.* [11] used numerical quadrature of the HF SCF equations to obtain results for several excited states of helium atoms and heliumlike ions over a range of magnetic fields up to 10^{12} G. The errors in this method, however, were best illustrated by later calculations of Jones, Ortiz, and Ceperley [12] who applied a basis set of Slater-type orbitals (STO) in solving the same equations, and were able to obtain lower energies for two excited states over many symmetries, but only up to magnetic field strengths of 10^{10} G. Later quantum Monte Carlo (QMC) calculations [13], using these same STO wave functions as a starting point, found that the residual basis set truncation errors were still significant over much of the range of magnetic-field strengths studied, and emphasized the need for more accurate HF wave functions. The helium spectrum in strong magnetic fields is the primary focus of this work. To more accurately determine the spectrum of neutral helium, we elected to stay within the basis set HF approach and utilize a much more flexible set of basis functions.

In this paper we use a basis set introduced by Aldrich and Greene [14] in combination with a systematic method for saturating the basis set [15] to study the lowest-energy electronic states of neutral helium. This basis set consists of functions of the form

$$\chi(\mathbf{r}) \propto \exp(-a\rho^2 - bz^2), \tag{1}$$

where a and b are variational parameters. This basis set has the advantage that it can be used to accurately represent states in which the charge density is highly anisotropic, where the values of the constants a and b differ. Combined with our previous method [12] for obtaining excited state solutions to the HF equations, we obtain three excitations for

each of the symmetries studied, with a precision that we estimate to be approximately 0.001 atomic energy units (hartree). We estimate the remaining basis set truncation error using our released-phase QMC method [13], which, in principle, is able to obtain the exact energies, including electron correlation. We also provide tables of dipole strengths calculated for the lowest three excitations of each symmetry, a necessity for accurate modeling of the absorptive behavior present in the atmospheres of strongly magnetized stars. In the first section we briefly review the methods employed in this study. The second section then presents our results, beginning with the HF energies and dipole matrix elements, and we consider the implications of our results for the adiabatic approximation. We also use stochastic methods to determine the correlation energy and estimate the remaining basis set truncation error in the HF energies. We conclude with some remarks about the applicability of our results to models of the atmospheres of magnetized compact stellar remnants.

II. METHOD

Our method, apart from the introduction of a different basis set, is essentially the same as that of our previous paper [12]. Here we recapitulate only the essential formulas. The magnetic field strength is parametrized by the constant $\beta_Z = \beta/Z^2 = B/B_0 Z^2$, where $B_0 = 4.701\times 10^9$ G $= 4701$ MG. The Hamiltonian in atomic units for an atom with N electrons and atomic number Z in constant magnetic field (along the z direction) is given by

$$\hat{\mathbb{H}} = \sum_{i=1}^{N}\left[-\frac{\nabla_i^2}{2} - \frac{Z}{r_i} + \frac{(Z^2\beta_Z)^2}{2}(x_i^2+y_i^2)\right] + Z^2\beta_Z(L_z+2S_z) + \sum_{1\le i<j\le N}\frac{1}{r_{ij}}, \tag{2}$$

where $L_z = \Sigma_{i=1}^N l_{iz}$ and $S_z = \Sigma_{i=1}^N s_{iz}$ are the z component of the total angular momentum and spin of the system, respectively, and lengths are in units of the Bohr radius a_0. Here we neglect contributions arising from the finite nuclear mass. We have chosen the magnetic field to be parallel to the z axis, and the symmetric gauge, which has vector potential $\mathbf{A} = B(-y,x,0)/2$. In the absence of external fields the eigenvalues of L^2, L_z, S^2, S_z, and parity, Π, are good quantum numbers. When the magnetic field is turned on, the rotational invariance is broken and the only conserved quantum numbers are the eigenvalues of L_z, S^2, S_z, and Π (alternatively, we will use the z parity, Π_z). We will use both the zero-field notation, and also the triplet of proper quantum numbers M (the eigenvalue of L_z), π_z and S_z in the form (M,π_z,S_z). Taking our wave function Ψ to be a single Slater determinant and minimizing the energy of the above Hamiltonian with respect to the electronic spin orbitals, $\{\psi_a\}$ [$\psi_a(\mathbf{x}) = \alpha(s)\otimes\phi_a(\mathbf{r})$, where $\alpha(s)$ is a spin function, $\phi_a(\mathbf{r})$ a spatial orbital, and $\mathbf{x} = (s,\mathbf{r})$], we obtain the usual Hartree-Fock equations,

$$F\psi_a = \epsilon_a\psi_a, \tag{3}$$

where F is the single-particle Fock operator,

$$F = h(\mathbf{r}) + \sum_b (\mathcal{J}_b - \mathcal{K}_b), \tag{4}$$

and

$$h(\mathbf{r}) = -\frac{1}{2}\nabla^2 - \frac{Z}{r} + \frac{(Z^2\beta_Z)^2}{2}(x^2+y^2) + Z^2\beta_Z(l_z+2s_z),$$

$$\mathcal{J}_b\psi_a = \left[\int d\mathbf{x}'|\mathbf{r}-\mathbf{r}'|^{-1}\psi_b^*(\mathbf{x}')\psi_b(\mathbf{x}')\right]\psi_a(\mathbf{x}), \tag{5}$$

$$\mathcal{K}_b\psi_a = \left[\int d\mathbf{x}'|\mathbf{r}-\mathbf{r}'|^{-1}\psi_b^*(\mathbf{x}')\psi_a(\mathbf{x}')\right]\psi_b(\mathbf{x}).$$

Note that we are still considering the integrals over the spin degrees of freedom for the direct, $\mathcal{J}$, and exchange, $\mathcal{K}$, integrals. We expand each spatial electronic orbital in a basis set, $\{\chi_\mu(\mathbf{r})\}$, of our choosing,

$$\phi_a(\mathbf{r}) = \sum_{\mu=1}^{N_b} c_{a\mu}\chi_\mu(\mathbf{r}), \tag{6}$$

where N_b is the number of basis set elements. We have chosen to use the basis set of Aldrich and Greene [14]

$$\chi_\mu(\rho,\varphi,z) = N_\mu\rho^{|m_\mu|}z^{p_\mu}e^{-im_\mu\varphi}e^{-a_\mu\rho^2-b_\mu z^2}, \tag{7}$$

where m_μ denotes the angular momentum quantum number of operator l_z, and $p_\mu = 0$ for positive z-parity states, and $p_\mu = 1$ for negative z-parity states. The parameters a_μ and b_μ allow for different treatment of the transverse and longitudinal distance dependence, a crucial consideration when the applied magnetic field gets strong enough that the atom tries to minimize the diamagnetic contribution to the total energy. Analytic expressions can be worked out for most of the matrix elements, while the nuclear repulsion [14] and electron-electron matrix elements can be reduced to one-dimensional integrals that are performed numerically. Our expressions for the electron-electron matrix elements can be found in the Appendix.

Our present calculations restrict the orbitals to have a common spatial dependence for two electrons in the same state but of opposite spin. In other words we use the restricted Hartree-Fock (RHF) approach. Details of how we achieve the solution in this method can be found in Ref. [12].

A. Even-tempered Gaussians

An important concern in Eq. (6) is whether or not the basis set is sufficiently well converged for a desired level of accuracy in the atomic total energy. Previous calculations [12] have been plagued by an inadequate basis set—even the largest basis sets used have not been well converged in a systematic way. In this work we have used even-tempered Gaussian (ETG) sequences [15] to systematically saturate the basis set for each electronic orbital. Essentially this means that a sequence of N_s, a, and b parameters are generated in such a way that they fill the possible range of values as each sequence is made longer (N_s increases). In zero-field calculations only one sequence of spheroidal Gaussians is needed

for each angular momentum type (for Gaussian type orbitals, $a=b$, and the Gaussian is multiplied by a spherical harmonic). These sequences of basis elements are given by

$$b_i = b_1 \delta_b^{i-1}, \quad i=1,\ldots,N_s, \tag{8}$$

where b_1 and δ_b are the variational parameters for the entire sequence that must be optimized with respect to the HF total energy. As N_s gets longer, the basis set saturates, or becomes more and more complete. These sequences have been successfully used for well saturated zero-field atomic calculations [15], a case in which the parameters a and b are equal. It should be emphasized that these ETG sequences are simply a reliable way in which the basis set can be saturated. In practice, we fully optimize the values of the basis set parameters for each value of N_s, the length of the sequences, with respect to the total energy. One can then also fit the resulting optimal parameters in order to obtain a scheme for extrapolating to even larger basis set sizes (sequence lengths) [15]. However, we have not done this extrapolation procedure, as the optimal sequences are sufficiently well converged in energy to meet our requirements for the accuracy of the total energy.

The main complication in the present application is that our basis set [Eq. (7)] is designed to break spherical symmetry ($a \neq b$), such that we have two parameters in each Gaussian basis function, separately describing the longitudinal and transverse directions. To compensate for this separation, we use a series of such ETG sequences, with the longitudinal parameters given by Eq. (8), and the matching transverse parameters given by

$$a_i = f b_i, \quad i=1,\ldots,N_s, \tag{9}$$

where f is a constant factor. We have typically selected f such that we use a series of 2–5 even-tempered sequences for each orbital, with $f=1,2,4,8,\ldots$. Note that the total number of basis functions is N_s multiplied by the number of different sequences. Additionally we have included a sequence such that a is fixed, $a=a_B$, where $a_B=Z^2\beta_Z/2$ is the exponential parameter for the first Landau level of an electron in a constant magnetic field. As the magnetic field gets larger, this Landau-level sequence becomes more and more important in the basis set expansion of the electronic orbitals. The adiabatic approximation corresponds to using only sequences in which a is fixed to a_B. We will explore this issue further below.

III. RESULTS

Our desired accuracy for the HF total energies is 0.001 hartree, such that we can resolve transitions in the optical regime with a precision of $\delta\lambda \lesssim 100$ Å, where $\lambda = hc/|E_i - E_f|$ is the wavelength of allowed transitions between initial and final states. Our RHF calculations reported here used a minimum of 2 ETG sequences for each orbital, with some calculations using up to 5 sequences. The convergence of the total energy as a function of the number of sequences was carefully checked at several different magnetic-field strengths (typically $\beta_Z=1,10,100$), and was converged to within 0.0005 hartree. It was necessary to include the Landau-level sequence ($a_i=a_B$) for the $1s$ orbital for $\beta_Z \gtrsim 1$, while it was always necessary (apart from $\beta_Z=0$) to include the Landau-level sequence for the second electronic orbital, due to the much greater impact of the applied field on the outermost electron. We began calculations with each sequence having a length of four [$N_s=4$ in Eq. (8)] and fully optimized the parameters for each sequence (two parameters for each sequence). This process was repeated until the energy converged within 0.0001 hartree, which typically required a length of $N_s=6$–8. A typical example of this behavior is shown in Fig. 1 for the first and third (inset) states of symmetry $(M,\pi_z,S_z)=(0,+,-1)$. The total energy in this example is amply converged by $N_s=7$. Note that we have chosen more stringent cutoffs for the convergence of the total energy with respect to the number and length of ETG sequences; thus the desired accuracy of 0.001 hartree is a conservative estimate of the remaining basis set truncation error.

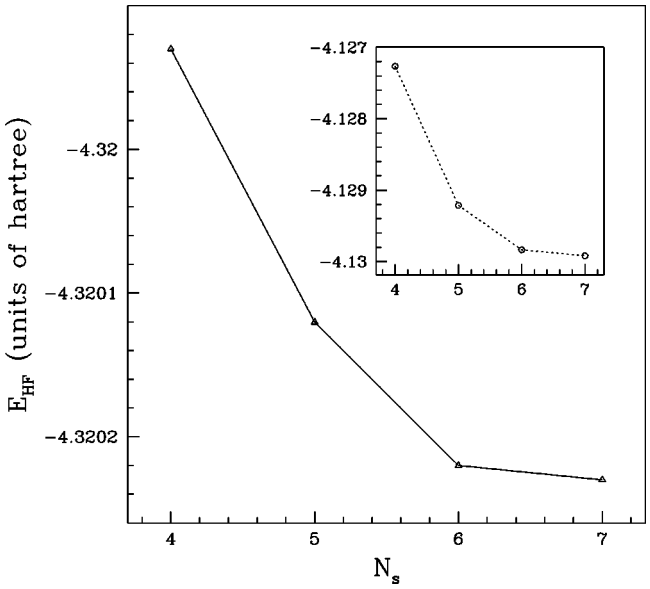

FIG. 1. Sample convergence of the first and third (inset) states of $(M,\pi_z,S_z)=(0,+,-1)$ symmetry ($1s2s$ and $1s4s$ at zero field) at $\beta_Z=1$.

A. Excited-state spectrum of neutral He

Tables I–VIII contain the HF-ETG energies computed according to the method outlined above, for the spin-polarized ($S_z=-1$) symmetries having $M=0,-1,-2,-3$, and $\pi_z=\pm$. We note that these energies are always lower than the best previously published HF results [12], with the exception of some of the very lowest states of each symmetry at small applied magnetic-field strength. This slight degradation (generally around 0–3×10^{-4} hartree) is due to the ETG basis functions not representing the correct cusp behavior [16] at the nucleus, while the Slater-type orbitals do possess a nonzero derivative at the origin. The ETG basis elements are much better, however, at reproducing the highly anisotropic behavior at high magnetic fields. This improved accuracy is reflected in the fact that the higher excited states are much superior to those published previously [12].

The spectrum of the energy states computed thus far is shown in Fig. 2. We note that the most tightly bound states

TABLE I. HF-ETG total energies for the first three excited states of $(M,\pi_z,S_z)=(0,+,-1)$ symmetry. Zero-field quantum numbers are given at the top of each column.

β_Z	$1s2s$	$1s3s$	$1s4s$
0.01	−2.2425	−2.1199	−2.0825
0.05	−2.4111	−2.2789	−2.2354
0.10	−2.5720	−2.4425	−2.4034
0.20	−2.8659	−2.7363	−2.6986
0.30	−3.1211	−2.9879	−2.9498
0.40	−3.3444	−3.2078	−3.1696
0.50	−3.5435	−3.4041	−3.3653
0.60	−3.7239	−3.5820	−3.5428
0.70	−3.8894	−3.7453	−3.7054
0.80	−4.0427	−3.8967	−3.8567
0.90	−4.1857	−4.0379	−3.9978
1.00	−4.3202	−4.1708	−4.1299
2.00	−5.3680	−5.2080	−5.1656
3.00	−6.1260	−5.9592	−5.9161
5.00	−7.2543	−7.0792	−7.0349
7.00	−8.1147	−7.9344	−7.8891
10.00	−9.1385	−8.9525	−8.9061
20.00	−11.4945	−11.2975	−11.2494
30.00	−13.1223	−12.9189	−12.8703
50.00	−15.4668	−15.2553	−15.2057
70.00	−17.2046	−16.9879	−16.9382
100.00	−19.2286	−19.0072	−18.9543

TABLE II. HF-ETG total energies for the first three excited states of $(0,-,-1)$ symmetry. Zero-field quantum numbers are given at the top of each column.

β_Z	$1s2p_0$	$1s3p_0$	$1s4p_0$
0.01	−2.2031	−2.1105	−2.0724
0.05	−2.4197	−2.2747	−2.2330
0.10	−2.6347	−2.4537	−2.4067
0.20	−2.9827	−2.7592	−2.7060
0.30	−3.2657	−3.0155	−2.9587
0.40	−3.5068	−3.2377	−3.1784
0.50	−3.7186	−3.4355	−3.3740
0.60	−3.9082	−3.6144	−3.5512
0.70	−4.0808	−3.7786	−3.7137
0.80	−4.2394	−3.9303	−3.8644
0.90	−4.3864	−4.0725	−4.0052
1.00	−4.5282	−4.2056	−4.1417
2.00	−5.5978	−5.2446	−5.1774
3.00	−6.3621	−5.9965	−5.9278
5.00	−7.4932	−7.1163	−7.0465
7.00	−8.3523	−7.9708	−7.9004
10.00	−9.3724	−8.9875	−8.9169
20.00	−11.7170	−11.3306	−11.2599
30.00	−13.3364	−12.9503	−12.8802
50.00	−15.6691	−15.2855	−15.2150
70.00	−17.3996	−17.0169	−16.9469
100.00	−19.4150	−19.0335	−18.9634

TABLE III. HF-ETG total energies for the first three excited states of $(-1,+,-1)$ symmetry. Zero-field quantum numbers are given at the top of each column.

β_Z	$1s2p_{-1}$	$1s3p_{-1}$	$1s4p_{-1}$
0.01	−2.2353	−2.1220	−2.0888
0.05	−2.5366	−2.2972	−2.2413
0.10	−2.8301	−2.4855	−2.4178
0.20	−3.3016	−2.8006	−2.7188
0.30	−3.6842	−3.0630	−2.9735
0.40	−4.0107	−3.2897	−3.1938
0.50	−4.2980	−3.4903	−3.3909
0.60	−4.5560	−3.6743	−3.5707
0.70	−4.7911	−3.8411	−3.7343
0.80	−5.0078	−3.9954	−3.8858
0.90	−5.2107	−4.1388	−4.0276
1.00	−5.4000	−4.2742	−4.1605
2.00	−6.8666	−5.3261	−5.1995
3.00	−7.9213	−6.0856	−5.9508
5.00	−9.4882	−7.2156	−7.0714
7.00	−10.6816	−8.0768	−7.9268
10.00	−12.1011	−9.1010	−8.9451
20.00	−15.3690	−11.4589	−11.2906
30.00	−17.6289	−13.0873	−12.9120
50.00	−20.8876	−15.4327	−15.2490
70.00	−23.3066	−17.1710	−16.9822
100.00	−26.1264	−19.1943	−18.9999

TABLE IV. HF-ETG total energies for the first three excited states of $(-1,-,-1)$ symmetry. Zero-field quantum numbers are given at the top of each column.

β_Z	$1s3d_{-1}$	$1s4d_{-1}$	$1s5d_{-1}$
0.01	−2.1403	−2.0903	−2.0673
0.05	−2.3512	−2.2588	−2.2271
0.10	−2.5528	−2.4382	−2.4012
0.20	−2.8938	−2.7436	−2.7010
0.30	−3.1698	−2.9990	−2.9541
0.40	−3.4065	−3.2211	−3.1745
0.50	−3.6156	−3.4184	−3.3709
0.60	−3.8036	−3.5969	−3.5487
0.70	−3.9753	−3.7606	−3.7119
0.80	−4.1335	−3.9122	−3.8629
0.90	−4.2806	−4.0538	−4.0038
1.00	−4.4193	−4.1908	−4.1372
2.00	−5.4881	−5.2306	−5.1733
3.00	−6.2545	−5.9827	−5.9240
5.00	−7.3900	−7.1035	−7.0426
7.00	−8.2528	−7.9582	−7.8968
10.00	−9.2773	−8.9754	−8.9134
20.00	−11.6315	−11.3192	−11.2567
30.00	−13.2562	−12.9403	−12.8772
50.00	−15.5955	−15.2756	−15.2123
70.00	−17.3302	−17.0081	−16.9442
100.00	−19.3495	−19.0247	−18.9603

TABLE V. HF-ETG total energies for the first three excited states of $(-2,+,-1)$ symmetry. Zero field quantum numbers are given at the top of each column.

β_Z	$1s3d_{-2}$	$1s4d_{-2}$	$1s5d_{-2}$
0.01	−2.1659	−2.0990	−2.0742
0.05	−2.4320	−2.2801	−2.2356
0.10	−2.6871	−2.4680	−2.4120
0.20	−3.1005	−2.7822	−2.7141
0.30	−3.4394	−3.0438	−2.9685
0.40	−3.7309	−3.2701	−3.1902
0.50	−3.9890	−3.4709	−3.3873
0.60	−4.2215	−3.6524	−3.5657
0.70	−4.4342	−3.8187	−3.7288
0.80	−4.6306	−3.9725	−3.8814
0.90	−4.8134	−4.1162	−4.0229
1.00	−4.9866	−4.2549	−4.1558
2.00	−6.3268	−5.3073	−5.1947
3.00	−7.2952	−6.0671	−5.9467
5.00	−8.7385	−7.1975	−7.0674
7.00	−9.8406	−8.0594	−7.9229
10.00	−11.1540	−9.0844	−8.9411
20.00	−14.1875	−11.4426	−11.2871
30.00	−16.2905	−13.0715	−12.9091
50.00	−19.3286	−15.4169	−15.2460
70.00	−21.5954	−17.1561	−16.9805
100.00	−24.2283	−19.1800	−18.9982

TABLE VI. HF-ETG total energies for the first three excited states of $(-2,-,-1)$ symmetry. Zero-field quantum numbers are given at the top of each column.

β_Z	$1s4f_{-2}$	$1s5f_{-2}$	$1s6f_{-2}$
0.01	−2.1201	−2.0829	−2.0636
0.05	−2.3268	−2.2521	−2.2241
0.10	−2.5299	−2.4317	−2.3985
0.20	−2.8637	−2.7372	−2.6990
0.30	−3.1378	−2.9933	−2.9522
0.40	−3.3738	−3.2149	−3.1726
0.50	−3.5823	−3.4142	−3.3690
0.60	−3.7702	−3.5933	−3.5469
0.70	−3.9417	−3.7577	−3.7100
0.80	−4.1000	−3.9096	−3.8610
0.90	−4.2473	−4.0513	−4.0020
1.00	−4.3861	−4.1853	−4.1353
2.00	−5.4573	−5.2258	−5.1717
3.00	−6.2263	−5.9786	−5.9225
5.00	−7.3654	−7.0998	−7.0416
7.00	−8.2310	−7.9553	−7.8957
10.00	−9.2549	−8.9729	−8.9126
20.00	−11.6182	−11.3183	−11.2562
30.00	−13.2459	−12.9392	−12.8766
50.00	−15.5879	−15.2748	−15.2119
70.00	−17.3240	−17.0073	−16.9441
100.00	−19.3448	−19.0248	−18.9605

TABLE VII. HF-ETG total energies for the first three excited states of $(-3,+,-1)$ symmetry. Zero-field quantum numbers are given at the top of each column.

Nβ_Z	$1s4f_{-3}$	$1s5f_{-3}$	$1s6f_{-3}$
0.01	−2.1406	−2.0914	−2.0651
0.05	−2.3923	−2.2721	−2.2320
0.10	−2.6344	−2.4587	−2.4085
0.20	−3.0275	−2.7726	−2.7110
0.30	−3.3511	−3.0339	−2.9655
0.40	−3.6294	−3.2598	−3.1872
0.50	−3.8759	−3.4606	−3.3846
0.60	−4.0980	−3.6418	−3.5630
0.70	−4.3019	−3.8082	−3.7267
0.80	−4.4906	−3.9618	−3.8784
0.90	−4.6669	−4.1056	−4.0200
1.00	−4.8318	−4.2444	−4.1532
2.00	−6.1195	−5.2967	−5.1919
3.00	−7.0517	−6.0567	−5.9443
5.00	−8.4426	−7.1872	−7.0654
7.00	−9.5058	−8.0493	−7.9220
10.00	−10.7734	−9.0743	−8.9396
20.00	−13.7044	−11.4330	−11.2861
30.00	−15.7378	−13.0624	−12.9073
50.00	−18.6784	−15.4083	−15.2443
70.00	−20.8674	−17.1463	−16.9778
100.00	−23.4342	−19.1738	−18.9986

TABLE VIII. HF-ETG total energies for the first three excited states of $(-3,-,-1)$ symmetry. Zero field quantum numbers are given at the top of each column.

β_Z	$1s5g_{-3}$	$1s6g_{-3}$	$1s7g_{-3}$
0.01	−2.1089	−2.0783	−2.0534
0.05	−2.3120	−2.2476	−2.2225
0.10	−2.5133	−2.4275	−2.3976
0.20	−2.8451	−2.7332	−2.6975
0.30	−3.1181	−2.9895	−2.9505
0.40	−3.3530	−3.2120	−3.1713
0.50	−3.5607	−3.4103	−3.3678
0.60	−3.7479	−3.5897	−3.5457
0.70	−3.9189	−3.7539	−3.7090
0.80	−4.0770	−3.9060	−3.8602
0.90	−4.2282	−4.0478	−4.0014
1.00	−4.3664	−4.1818	−4.1341
2.00	−5.4393	−5.2229	−5.1707
3.00	−6.2096	−5.9759	−5.9216
5.00	−7.3514	−7.0976	−7.0410
7.00	−8.2188	−7.9533	−7.8953
10.00	−9.2476	−8.9714	−8.9121
20.00	−11.6106	−11.3173	−11.2552
30.00	−13.2408	−12.9382	−12.8765
50.00	−15.5847	−15.2745	−15.2119
70.00	−17.3216	−17.0066	−16.9440
100.00	−19.3436	−19.0249	−18.9606

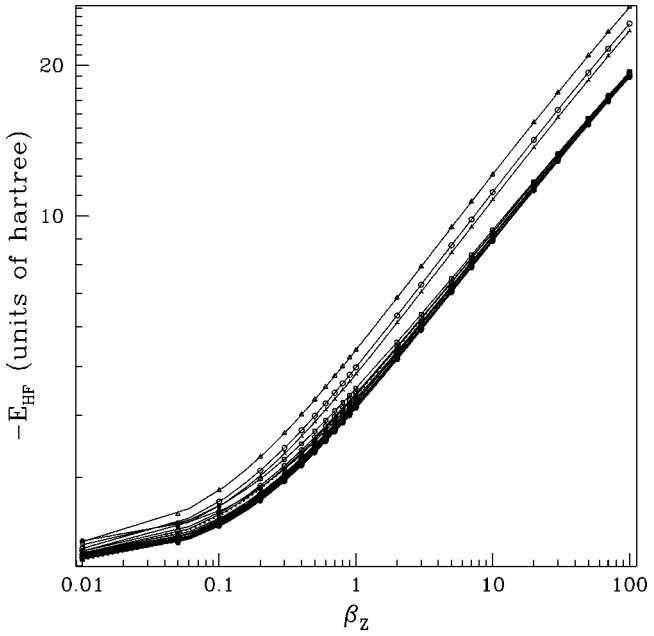

FIG. 2. The energy spectrum of 24 states of neutral helium in applied longitudinal magnetic fields up to $\beta_Z=100$, or approximately 2×10^{12} G.

[the first states of $(-1,+,-1),(-2,+,-1),(-3,+,-1)$ symmetry] lie lowest in energy, by a considerable margin, with a gap to higher excitations that increases monotonically with applied field strength. The remaining states form a broad band of excitations whose width is slowly increasing as a function of magnetic-field strength. It should be noted that many additional tightly bound states lie between the band of excitations and the lowest tightly bound $(-3,+,-1)$ state, for example, $(-4,+,-1),(-5,+,-1),\ldots$. We have chosen to focus on the most energetically favorable states at high magnetic fields. Thus we have considered only spin triplet states, and have restricted ourselves to states with $-3\leqslant M\leqslant 0$. If it is necessary to compute more symmetries to accurately model magnetized white dwarf atmospheres, it is a simple matter to extend the calculations presented in this work.

B. Dipole strengths for low-lying He transitions

The dipole matrix element, in atomic units, between initial state Ψ_i and final state Ψ_f is given by

$$d_{if}=\sum_{j=1}^{2}\langle\Psi_i|\sqrt{\frac{4\pi}{3}}r_jY_{1,\Delta M}|\Psi_f\rangle, \tag{10}$$

where $\Delta M=M_f-M_i$, and $Y_{1,\Delta M}$ is the usual spherical harmonic. These dipole matrix elements vanish unless the zero field angular momentum quantum numbers (eigenvalues of the operator L^2) differ by one, $|L_f-L_i|=1$. This same rule also applies at nonzero applied field, as the diamagnetic term only couples states that differ by two in L. These selection rules allow for ten possible transitions between states of different symmetry (that we have considered). Numerical tables for the dipole matrix elements can be provided by the authors upon request, or obtained on the World Wide Web [17]. Graphical results for the dipole matrix elements are shown in Fig. 3. The ninety allowed transitions plotted in Fig. 3 show some basis set truncation error, which is not unexpected, as the HF-SCF wave-functions are optimized according to energy, leaving other expectation values more sensitive to the basis set error.

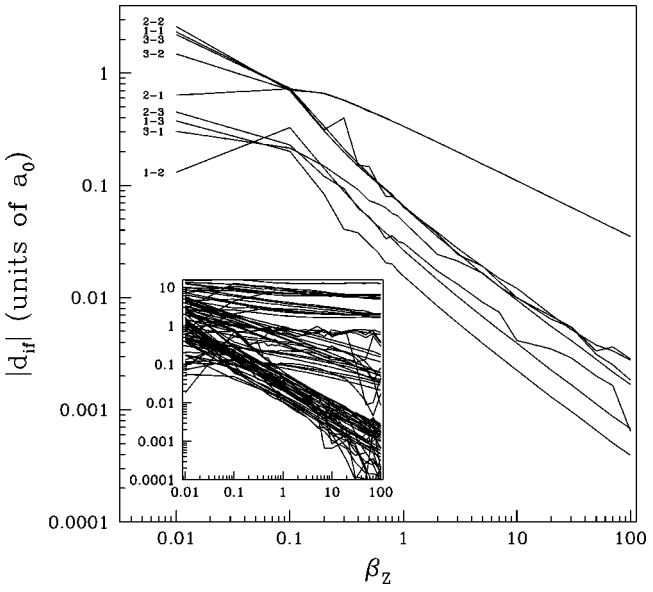

FIG. 3. Dipole strengths for allowed transitions in neutral helium as a function of magnetic-field strength. The main figure shows the transitions from symmetry $(M,\pi_z,S_z)=(-1,+,-1)$ to $(0,+,-1)$, with labels denoting the level of excitation. For example, 1-1 is the transition between zero-field states $1s2p_{-1}$ and $1s2s$. The inset shows all of the data for all eight symmetries that we have considered, for a total of 90 transitions.

C. Validity of the adiabatic approximation

In the often used adiabatic approximation [5], the only basis functions used are those corresponding to the lowest Landau level, while the functional dependence in the longitudinal direction is allowed to vary. We assess the validity of such an approximation by measuring the relative average transverse ''widths'' of the electron orbitals, namely,

$$\langle\phi_2|x^2+y^2|\phi_2\rangle/\langle\phi_1|x^2+y^2|\phi_1\rangle=\frac{\langle\rho^2\rangle_2}{\langle\rho^2\rangle_1}, \tag{11}$$

where ϕ_1 corresponds to the first $(1s)$ orbital, and ϕ_2 the second, excited-state, orbital. If the adiabatic approximation is valid, this ratio of the widths of the second electron compared to the first should approach a constant [see Eq. (14)]. We show examples of this width for the $1s2p_{-1}$, $1s3p_{-1}$, and $1s4p_{-1}$ states in Fig. 4. The lower panel shows the width for all values of the applied magnetic field, while the upper panel focuses on the region where $\beta_Z\gtrsim1$. We note that the ratio only approaches a constant for the very largest field strengths, $\beta_Z\gtrsim80$–100, and is still slowly varying even in this superstrong field regime. The ratio is also only slightly dependent on the degree of excitation.

We can learn more by examining separately the behavior of each of the two electronic orbitals. In the limit of infinite magnetic-field strength, the electrons should occupy the lowest Landau level,

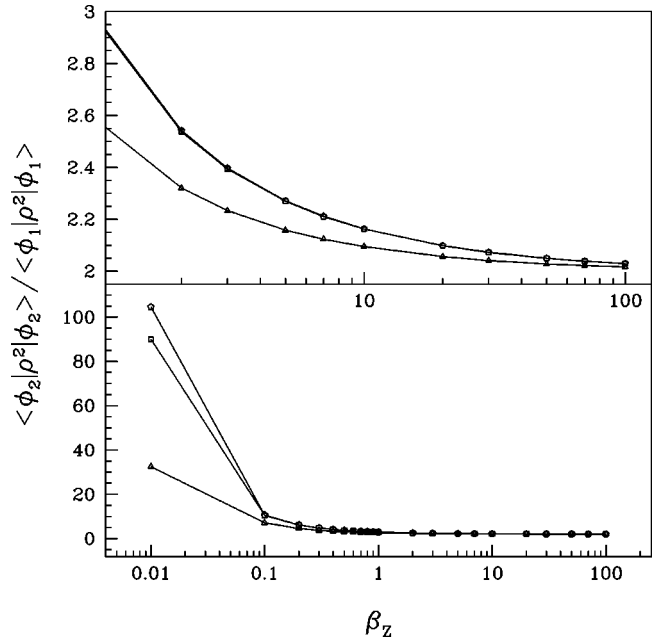

FIG. 4. The ratio of the expectation value of ρ^2 for the second electronic orbital relative to the first for the first three excited states of $(M,\pi_z,S_z)=(-1,+,-1)$ symmetry. The upper panel is a close up of the data for larger field strengths. The ratio should approach 2.0 in the adiabatic limit. Lines are provided only as a guide to the eye.

$$\Phi_{nm}^{Lan}(\rho,\varphi)=\frac{\sqrt{n!}}{\sqrt{2\pi(n+|m|)!\,l^2}}\left(\frac{\rho}{\sqrt{2}l}\right)^{|m|}\times L_n^{|m|}\left(\frac{\rho^2}{l^2}\right)e^{-im\varphi}e^{-\rho^2/4l^2}, \tag{12}$$

where $l=\sqrt{1/2\beta}$ is the magnetic length, and $L_n^{|m|}$ is an associated Laguerre polynomial. For the lowest Landau state, $n=0$, and we have

$$\Phi_{0m}^{Lan}=\left[\frac{2}{2\pi|m|!}\right]^{1/2}\beta^{\frac{|m|+1}{2}}\rho^{|m|}e^{-\beta\rho^2/2}e^{-im\varphi}. \tag{13}$$

The full wave function also includes a factor of an unknown function of z times the cylindrical Landau state, but we are concerned here with the quality of the adiabatic approximation, so we focus only on the accuracy of the description of the transverse behavior. Now we consider the expectation value of ρ^2 in the lowest Landau orbitals,

$$\langle\Phi_{0m}^{Lan}|\rho^2|\Phi_{0m}^{Lan}\rangle=\frac{|m|+1}{\beta}=\frac{|m|+1}{Z^2\beta_Z}. \tag{14}$$

We see that, in the adiabatic limit, the expectation value of ρ^2 for each electronic orbital should be a simple constant divided by the magnetic-field strength. Figures 5 and 6 plot this expectation value as a function of $1/\beta_Z$ for the same example states that we considered above, the $1s2p_{-1}$, $1s3p_{-1}$, and $1s4p_{-1}$ states. Figure 5 plots $\langle\rho^2\rangle$ for the first electronic orbital of helium (the $1s$ state at zero magnetic field), while Fig. 6 shows the same result for the

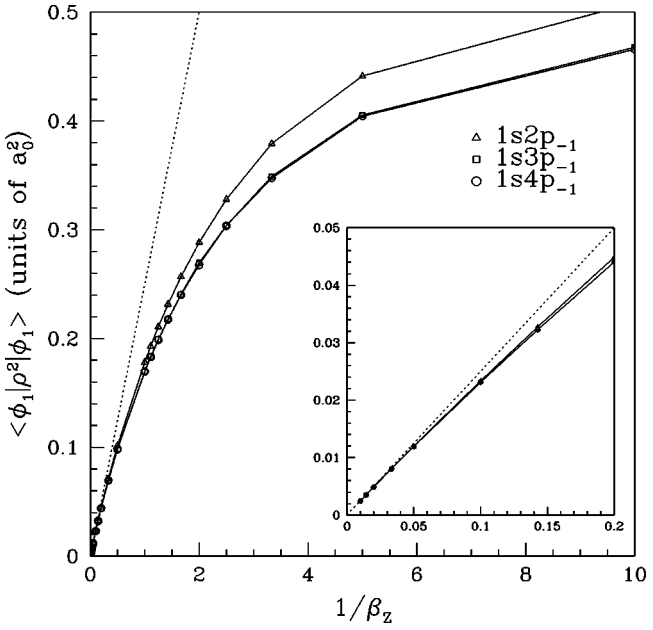

FIG. 5. The expectation value of ρ^2 for the first HF electronic orbital ϕ_1 as a function of magnetic-field strength, which should become linear in the limit when the adiabatic approximation is valid. Three orbitals are shown, corresponding to the first three excitations of $(M,\pi_z,S_z)=(-1,+,-1)$ symmetry. The inset shows a close up of the superstrong field regime near the origin. The dashed line indicates the adiabatic limit. Solid lines are provided only as a guide to the eye.

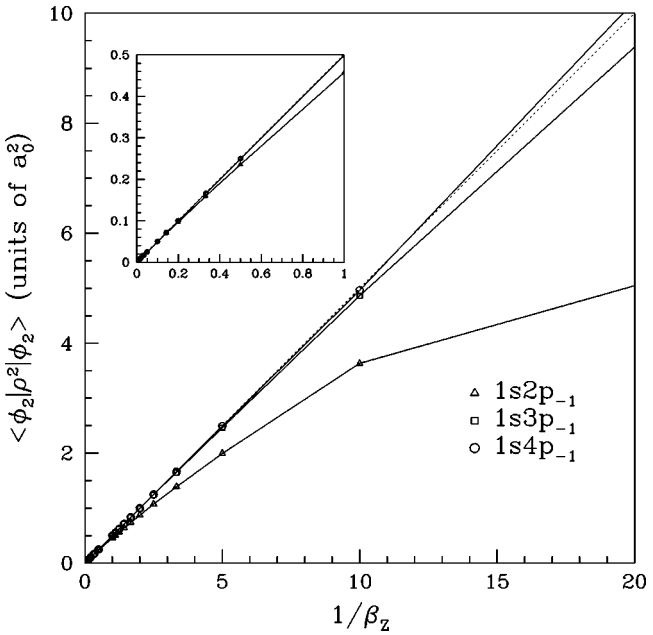

FIG. 6. The expectation value of ρ^2 for the second (excited) HF electronic orbital ϕ_2 as a function of magnetic-field strength, which should become linear in the limit when the adiabatic approximation is valid. Three orbitals are shown, corresponding to the first three excitations of $(M,\pi_z,S_z)=(-1,+,-1)$ symmetry. The inset shows a close up of the superstrong field regime near the origin. Solid lines are provided only as a guide to the eye. The dashed line indicates the adiabatic limit.

second orbital. We see in Fig. 5 that the approach to the adiabatic limit [indicated by the dashed line, whose slope is 1/4 by Eq. (14)] is really not valid until $\beta_Z \gtrsim 50$, a very large field indeed (about 10^{12} G). We also note that the limit is reached at approximately the same value of field strength for all three states, a reasonable result, as the innermost electron should not be greatly different from one excited state to the next. The second orbital, however, reaches the adiabatic limit much more quickly, as we see from Fig. 6. The more spatially extended states feel a much larger effective magnetic field (due to the diamagnetic term in the Hamiltonian); thus the tightly bound $2p_{-1}$ state (given by the triangles) reaches the adiabatic limit (indicated by the dashed line of slope 1/2) more slowly ($\beta_Z \simeq 5$) than the next two excited states, which are very near the adiabatic regime at $\beta_Z \simeq 0.1$–0.2. The implications of these results for multielectron atoms is that the adiabatic approximation is not good for the innermost electrons, except at extremely large field strengths, due to the importance of the Coulomb repulsion from the nucleus. Thus we conclude that the adiabatic approximation for multielectron atoms is seldom very accurate, even for the large magnetic fields found in magnetized white dwarfs and neutron stars, which are generally less than 10^{12} G.

D. Basis set truncation error and correlation energy

To provide an estimation of the size of our basis set truncation error, we have used two quantum Monte Carlo methods. The fixed-phase method [18] (FPQMC) is a variational method that projects out the ground state of a particular symmetry using stochastic random walks. If the state were bosonic, FPQMC would yield an exact result (albeit with statistical error bars) for the total energy. Since we have fermions, the FPQMC energies are an upper bound to the exact total energy (often a very good upper bound) for the ground state of a given symmetry, whose quality is constrained by the fixed-phase approximation. The released-phase method [13] (RPQMC) is an ''exact'' method that can simultaneously determine the ground and excited states by using correlation functions in imaginary time. If sufficiently well converged in imaginary time, this RPQMC method obtains the exact energies, but always provides at least an upper bound to the exact excited-state energies. Both of these methods, along with an earlier application to low-lying excited states of helium (for smaller and somewhat inferior STO basis sets), are reviewed in Ref. [19]. It is difficult, of course, to separate out the basis set truncation errors from the correlation energy,

$$E_C = E_{HF} - E_{QMC}. \tag{15}$$

Our ETG basis set should be equally valid at all field strengths, hence we can look for basis set error by examining the behavior of the correlation energy as a function of field strength. Errors arising from truncation of the basis set should show up as (small) perturbations on the otherwise smooth correlation energy curve. The behavior of the correlation energy for the lowest state of each of the eight symmetries studied is shown in Fig. 7. From the small oscillations in the correlation energy curves we estimate, for the range of magnetic field strengths $0 \leqslant \beta_Z \leqslant 1$, that the truncation error is generally less than 0.001 hartree. For larger fields the truncation error increases. We note that E_C increases slowly with applied field strength, except for the most tightly bound states, which have zero-field quantum numbers $1s2p_{-1}$, $1s3d_{-2}$, and $1s4f_{-3}$, which increase rather dramatically as the field strength grows larger.

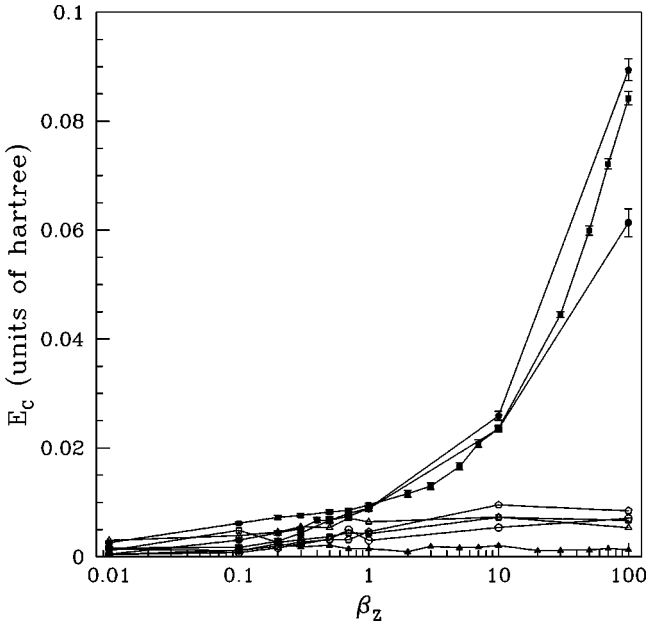

FIG. 7. The correlation energy from FPQMC as a function of magnetic-field strength for the lowest state of each symmetry corresponding to $S_z = -1$, $M = 0$ (triangles), $M = -1$ (squares), $M = -2$ (pentagons), and $M = -3$ (circles). The positive z-parity states have solid symbols. Lines are provided only as guides to the eye.

Table IX compares our current RPQMC results for a selected set of magnetic-field strengths and all eight symmetries studied with our previous RPQMC results [13]. We note that the previous results suffered from poor wave-function quality, as the present results (the method, when insufficiently converged in imaginary time, remains variational) are greatly improved, especially for the higher excitations. We also note that the correlation energy is quite small for the highest excitations, regardless of the symmetry state. This reduction in correlation energy for the highest excitations is most likely due to the large physical separation between the innermost and outermost electrons.

E. Comparison with other calculations

For our HF-ETG results we have already noted a favorable comparison with the best HF excited state calculations in the literature [12]. For our fully correlated RPQMC results we compare, in Table X, with the recent work of Scrinzi [20], who applied a variational calculation with a correlated basis to the first three excitations of $M = 0$ and $M = -1$, and Becken, Schmelcher, and Diakonos, who performed a very large configuration interaction (CI) calculation for the $M = 0$ symmetries, with up to six excited states. We note that our results compare favorably with the calculations of Becken, Schmelcher, and Diakonos at least for the symmetries that they have computed thus far, while there are large discrepancies with the results of Scrinzi. Some of Scrinzi's

TABLE IX. Comparison of released-phase QMC results, E_{RP}, with the current ETG Hartree-Fock energies E_{HF}^{ETG} and the best previous RP results from Ref. [13]. Blanks are left for the entries for which no previous RP calculations were done. Fixed-phase QMC results, E_{FP}, are also shown for the lowest excited state of each symmetry. We note that the previous RP results, Ref. [13], are considerably improved for the higher excitations, which reflect the higher quality of the present HF wave functions.

β_Z	$-E_{HF}^{ETG}$	Ref. [13]	$-E_{RP}$	$-E_{FP}$	$-E_{HF}^{ETG}$	Ref. [13]	$-E_{RP}$	$-E_{HF}^{ETG}$	Ref. [13]	$-E_{RP}$
			$1s2s$			$1s3s$			$1s4s$	
0.01	2.2425	2.2438(3)	2.2439(2)	2.2440(2)	2.1199	2.1209(1)	2.1206(3)	2.0825	2.0687(9)	2.0830(6)
0.10	2.5720	2.5737(3)	2.5738(2)	2.5731(3)	2.4425	2.4395(9)	2.4433(3)	2.4034	2.3497(21)	2.4034(4)
1.00	4.3202	4.3204(5)	4.3218(6)	4.3217(3)	4.1708	4.1169(19)	4.1716(9)	4.1299		4.1307(9)
			$1s2p_0$			$1s3p_0$			$1s4p_0$	
0.01	2.2031	2.2050(6)	2.2053(4)	2.2061(3)	2.1105	2.1100(3)	2.1116(2)	2.0724	2.0578(14)	2.0718(5)
0.10	2.6347	2.6397(9)	2.6395(5)	2.6385(3)	2.4537	2.4545(6)	2.4558(4)	2.4067	2.3925(7)	2.4077(4)
1.00	4.5283	4.5314(4)	4.5352(6)	4.5347(2)	4.2056	4.1651(8)	4.2067(7)	4.1417		4.1425(10)
			$1s2p_{-1}$			$1s3p_{-1}$			$1s4p_{-1}$	
0.01	2.2353	2.2380(9)	2.2384(3)	2.2380(2)	2.1220	2.1219(5)	2.1231(5)	2.0888	2.0809(9)	2.0898(3)
0.10	2.8295	2.8354(5)	2.8354(6)	2.8356(2)	2.4855	2.4856(5)	2.4869(11)	2.4178	2.3852(17)	2.4189(2)
1.00	5.4000	5.4072(13)	5.4101(22)	5.4096(3)	4.2742	4.2436(32)	4.2753(2)	4.1605		4.1608(8)
			$1s3d_{-1}$			$1s4d_{-1}$			$1s5d_{-1}$	
0.01	2.1403	2.1410(1)	2.1412(3)	2.1414(3)	2.0903	2.0912(2)	2.0912(2)	2.0673	2.0624(9)	2.0696(4)
0.10	2.5528	2.5590(27)	2.5583(18)	2.5577(4)	2.4382	2.4369(12)	2.4392(5)	2.4012	2.3504(14)	2.4022(4)
1.00	4.4193	4.4214(19)	4.4236(8)	4.4235(5)	4.1908	4.1074(9)	4.1919(6)	4.1372		4.1379(7)
			$1s3d_{-2}$			$1s4d_{-2}$			$1s5d_{-2}$	
0.01	2.1659		2.1667(2)	2.1664(2)	2.0990		2.0996(2)	2.0742		2.0751(4)
0.10	2.6871		2.6899(9)	2.6902(2)	2.4680		2.4691(14)	2.4120		2.4125(4)
1.00	4.9866		4.9941(9)	4.9956(5)	4.2549		4.2565(21)	4.1558		4.1567(5)
			$1s4f_{-2}$			$1s5f_{-2}$			$1s6f_{-2}$	
0.01	2.1201		2.1198(8)	2.1206(1)	2.0829		2.0834(5)	2.0636		2.0655(6)
0.10	2.5299		2.5316(9)	2.5311(3)	2.4317		2.4326(3)	2.3985		2.3993(4)
1.00	4.3861		4.3888(22)	4.3907(5)	4.1853		4.1854(3)	4.1353		4.1356(1)
			$1s4f_{-3}$			$1s5f_{-3}$			$1s6f_{-3}$	
0.01	2.1406		2.1421(4)	2.1422(3)	2.0914		2.0920(7)	2.0651		2.0680(7)
0.10	2.6344		2.6330(22)	2.6361(4)	2.4587		2.4591(14)	2.4085		2.3980(8)
1.00	4.8318		4.8392(13)	4.8407(4)	4.2444		4.2459(9)	4.1532		4.1537(2)
			$1s5g_{-3}$			$1s6g_{-3}$			$1s7g_{-3}$	
0.01	2.1089		2.1095(3)	2.1094(2)	2.0783		2.0791(3)	2.0534		2.0544(12)
0.10	2.5133		2.5141(2)	2.5141(1)	2.4275		2.4281(2)	2.3976		2.3982(8)
1.00	4.3664		4.3714(18)	4.3694(4)	4.1818		4.1835(6)	4.1341		4.1349(6)

values for the total energy are considerably lower in energy than both our RPQMC results and the CI values. The agreement between the distinctly different CI and RPQMC methods is reassuring, and it seems most likely that these anomalously low energies of Scrinzi reflect numerical errors.

IV. CONCLUSIONS

We have applied a systematic method of basis-set saturation within the Hartree-Fock formalism for the case of neutral helium in strong magnetic fields, obtaining an accuracy of approximately 0.001 hartree atomic units over a wide range of magnetic-field strengths. The resulting accuracy in determining wavelengths for transitions among these states is thus $\delta\lambda/\lambda \lesssim 0.0021/\Delta E_{HF}$, for $\beta_Z \lesssim 1$. For optical transitions, this accuracy is $\lesssim 2\%$. Unfortunately, the dipole matrix elements also have truncation errors, which are much more difficult to estimate.

Using our accurate HF-ETG wave functions, we have

TABLE X. Comparison of fully correlated RPQMC energies, E_{RP}, with recent values found in the literature, where available. Values in parentheses for the RPQMC energies are statistical error bars. Those for Ref. [20] are estimated uncertainties in the last digit quoted. Zero-field quantum numbers are listed above each block of entries. All energies are in hartree atomic units.

β_Z	$-E_{RP}$	Ref. [20]	Ref. [21]	$-E_{RP}$	Ref. [20]	Ref. [21]	$-E_{RP}$	Ref. [20]	Ref. [21]
	$1s2s$			$1s3s$			$1s4s$		
0.01	2.2439(2)		2.243 958	2.1206(3)		2.121 107	2.0830(6)		2.087 409
0.10	2.5738(2)	2.57859(1)	2.573 615	2.4433(3)	2.4686(56)	2.443 352	2.4034(4)		2.403 631
	$1s2p_0$			$1s3p_0$			$1s4p_0$		
0.01	2.2053(4)		2.205 130	2.1116(2)		2.111 478	2.0718(5)		2.079 242
0.10	2.6395(5)	2.64014(0)	2.638 222	2.4558(4)	2.4944(90)	2.455 054	2.4077(4)	2.411(28)	2.407 425
	$1s2p_{-1}$			$1s3p_{-1}$			$1s4p_{-1}$		
0.01	2.2384(3)			2.1231(5)			2.0898(3)		
0.10	2.8354(6)	2.835 72(0)		2.4869(11)	2.5044(3)		2.4189(2)	2.396(45)	
	$1s3d_{-1}$			$1s4d_{-1}$			$1s5d_{-1}$		
0.01	2.1412(3)			2.0912(2)			2.0696(4)		
0.10	2.5583(18)	2.565 70(7)		2.4392(5)	2.437(14)		2.4022(4)		

used quantum Monte Carlo methods to determine the correlation energy (the difference between Hartree-Fock and the exact total energy) and estimate the residual basis set truncation energies. We have also evaluated the validity of the adiabatic approximation, and found that it is poor for the lowest-lying states and magnetic-field strengths. For example, the ground state of neutral helium does not enter the adiabatic regime until $\beta_Z \gtrsim 50$.

Both the dipole strengths and transition energies are required to construct a detailed model of the atmospheres of magnetic white dwarfs, which has not yet been done for stars suspected of containing neutral helium. We hope that the extensive tabulations provided in this work can provide meaningful input into such models. Tables of numerical results for both the dipole matrix elements and energies can be obtained on the World Wide Web [17].

ACKNOWLEDGMENTS

Calculations were performed at the National Center for Supercomputing Applications and the Cornell Theory Center. This work was performed under the auspices of the U.S. Department of Energy.

APPENDIX: ELECTRON-ELECTRON MATRIX ELEMENT

The strategy that we have used for the electron-electron matrix elements reduces the six-dimensional integral to a one-dimensional one that can be rapidly evaluated using standard numerical quadrature methods. The matrix elements between basis functions of the form of Eq. (7),

$$I^{ee}_{\mu\nu\lambda\sigma} = \left\langle \chi_\mu(\mathbf{r}_1)\chi_\lambda(\mathbf{r}_2) \left| \frac{1}{|\mathbf{r}_1-\mathbf{r}_2|} \right| \chi_\nu(\mathbf{r}_1)\chi_\sigma(\mathbf{r}_2) \right\rangle, \tag{A1}$$

can be expanded using the identity

$$\frac{1}{r_{12}} = \frac{1}{|\mathbf{r}_1-\mathbf{r}_2|} = \frac{1}{2\pi^2}\int_0^\infty du \int_{\mathbb{R}^3} d\mathbf{k}\; e^{i\mathbf{k}\cdot\mathbf{r}_{12}-k^2u}. \tag{A2}$$

We now expand the three dimensional integral over $\mathbf{k}$ in cylindrical coordinates k_ρ, k_z, and k_φ,

$$I^{ee}_{\mu\nu\lambda\sigma} = \delta_{m_1 m_2} N_{\mu\nu\lambda\sigma} \int_0^\infty du\; I_{k_\rho}(u) I_{k_z}(u), \tag{A3}$$

where $N_{\mu\nu\lambda\sigma} = N_\mu N_\nu N_\lambda N_\sigma$, $m_1 = m_\mu + m_\nu$, $m_2 = m_\lambda + m_\sigma$, and the remaining one-dimensional integral is evaluated numerically. The two expressions remaining in the integrand are the results from the integration over k_ρ and k_z.

$$\begin{aligned} I_{k_\rho}(u) = {} & \frac{\pi}{2^{2m_1+1}} \frac{(n_1+n_2+m_1)!}{a_1^{n_1+m_1+1} a_2^{n_2+m_1+1}} \\ & \times \frac{(u+1/4a_1)^{n_2}(u+1/4a_2)^{n_1}}{(u+A)^{n_1+n_2+m_1+1}} \\ & \times F\left(-n_2, -n_1; -n_2-n_1-m_1; \right. \\ & \left. \times \frac{u(u+A)}{(u+1/4a_1)(u+1/4a_2)} \right), \end{aligned} \tag{A4}$$

where $A = 1/[4(a_1+a_2)]$ and F is the confluent hypergeometric function, in this particular case a relatively simple finite series.

$$\begin{aligned} I_{k_z}(u) = {} & (-1)^p \frac{\pi^{3/2}}{8^p} b_1^{-p_1-1/2} b_2^{-p_2-1/2} p_1! p_2! (u+C)^{-p-1/2} \\ & \times \sum_{j_1=0}^{[p_1/2]} \sum_{j_2=0}^{[p_2/2]} \frac{(-1)^{j_1+j_2} b_1^{j_1} b_2^{j_2} (2p-2j_1-2j_2-1)!!}{j_1! j_2! (p_1-2j_1)! (p_2-2j_2)!} \\ & \times [2(u+C)]^{j_1+j_2}, \end{aligned} \tag{A5}$$

where $C=1/[4(b_1+b_2)]$ and the numbered quantities are related to the parameters of the original basis functions by

$$a_1=a_\mu+a_\nu, \quad a_2=a_\lambda+a_\sigma, \tag{A6}$$

$$b_1=b_\mu+b_\nu, \quad b_2=b_\lambda+b_\sigma, \tag{A7}$$

$$p_1=p_\mu+p_\nu, \quad p_2=p_\lambda+p_\sigma, \tag{A8}$$

$$n_1=(|m_\mu|+|m_\nu|-m_\mu-m_\nu)/2,$$

$$n_2=(|m_\lambda|+|m_\sigma|-m_\lambda-m_\sigma)/2, \tag{A9}$$

and $p_1+p_2=2p$ must be even (otherwise the integral $I^{ee}_{\mu\nu\lambda\sigma}$ is zero).

[1] J. D. Landstreet, in *Cosmical Magnetism*, edited by D. Lynden-Bell (Kluwer Academic, New York, 1994).
[2] W. Rosner, G. Wunner, H. Herold, and H. Ruder, J. Phys. B **17**, 29 (1984).
[3] H. Ruder, G. Wunner, H. Herold, and F. Geyer, *Atoms in Strong Magnetic Fields* (Springer, Berlin, 1994).
[4] G. D. Schmidt, W. B. Latter, and C. B. Foltz, Astrophys. J. **350**, 758 (1990); G. D. Schmidt, R. G. Allen, P. S. Smith, and J. Liebert, *ibid.* 463, 320 (1996).
[5] L. I. Schiff and H. Snyder, Phys. Rev. **55**, 59 (1939).
[6] R. Henry, R. F. O'Connell, E. R. Smith, G. Chanmugam, and A. J. Rajagopal, Phys. Rev. D **9**, 329 (1974); G. L. Surmelian, R. Henry, and R. F. O'Connell, Phys. Lett. **49A**, 431 (1974).
[7] M. Vincke and D. Baye, J. Phys. B **22**, 2089 (1989).
[8] M. V. Ivanov, J. Phys. B **27**, 4513 (1994).
[9] D. M. Larsen, Phys. Rev. B **20**, 5217 (1979).
[10] A. Scrinzi, J. Phys. B **29**, 6055 (1996).
[11] G. Thurner, H. Korbel, M. Braun, H. Herold, H. Ruder, and G. Wunner, J. Phys. B **26**, 4719 (1993).
[12] M. D. Jones, G. Ortiz, and D. M. Ceperley, Phys. Rev. A **54**, 219 (1996).
[13] M. D. Jones, G. Ortiz, and D. M. Ceperley, Phys. Rev. E **55**, 6202 (1997).
[14] C. Aldrich and R. L. Greene, Phys. Status Solidi B **93**, 343 (1979).
[15] M. W. Schmidt and K. Ruedenberg, J. Chem. Phys. **71**, 3951 (1979).
[16] T. Kato, Commun. Pure Appl. Math. **10**, 151 (1957).
[17] http://www.ncsa.uiuc.edu/Apps/CMP/papers/jon98/jon98.html
[18] G. Ortiz, D. M. Ceperley, and R. M. Martin, Phys. Rev. Lett. **71**, 2777 (1993).
[19] M. D. Jones, G. Ortiz, and D. M. Ceperley, Int. J. Quantum Chem. **64**, 523 (1997).
[20] A. Scrinzi, Phys. Rev. A **58**, 3879 (1998).
[21] W. Becken, P. Schmelcher, and F. K. Diakonos, J. Phys. B. (to be published day April 1999).